





18 **Abstract:** The lack of long-term and high-quality solar radiation data has been an  
19 obstacle for scientific and industrial fields. In this study, a dense station-based long-  
20 term and high-accuracy dataset of daily surface solar radiation was developed using  
21 two surface radiation models. One is the model developed by Yang et al. (2006) for  
22 global radiation estimation, and the other is the model developed by Tang et al. (2018)  
23 for direct radiation estimation. The main inputs for the development of the dataset are  
24 surface pressure, air temperature, relative humidity, horizontal visibility, and sunshine  
25 duration, which are the routine meteorological variables observed at the 2743 China  
26 Meteorological Administration (CMA) weather stations. Validation against in-situ  
27 observations and comparisons with two satellite-based radiation products show that our  
28 station-based radiation dataset clearly outperforms the satellite-based radiation  
29 products at both daily and monthly scales. In addition, our dataset is available for more  
30 than 60 years and includes three radiation components of global, direct and diffuse  
31 radiation, which is not possible with satellite products. This station-based radiation  
32 dataset will contribute to the climate change research and solar energy engineering  
33 applications in the future.

34 **Keywords:** Global radiation; Direct radiation; Diffuse radiation; High-accuracy; Long-  
35 term; Dataset.

36

37

38



## 39 **1. Introduction**

40 Solar radiation provides energy to everything on Earth, drives the water, energy  
41 and carbon cycles of the Earth's climate system, and largely determines the climatic  
42 conditions of human habitats (Wild et al., 2009). Therefore, solar radiation information  
43 at the Earth's surface is crucial in research of agriculture, hydrology, ecology, climate  
44 change, and simulations of land surface processes (Wang et al., 2012). Solar radiation  
45 reaching the horizontal surface is called as total solar radiation or global radiation ( $R_g$ ),  
46 and is composed of direct radiation ( $R_{dir}$ ) and diffuse radiation ( $R_{dif}$ ). Global radiation  
47 is an important component of the surface energy budgets (Wild et al., 2015), and  
48 accurate global radiation data will contribute to the simulation of land surface-related  
49 processes, such as ecological, hydrological, agricultural, and glacial simulations (Tang  
50 et al., 2019a). In addition, both direct and diffuse radiation provide energy for plant  
51 photosynthesis and transpiration, and are essential for hydrological and agricultural  
52 studies (Lee et al., 2017). Due to its multidirectional nature, diffuse radiation penetrates  
53 in the vegetation canopy more than direct radiation, and more diffuse radiation can  
54 increase light energy use efficiency of the canopy (Mercado et al., 2009, Yang et al.,  
55 2019). For example, under the same global radiation condition, increasing the  
56 proportion of diffuse radiation can increase the light energy use efficiency of different  
57 vegetation types by 6-180% (Gu et al., 2002; Alton et al., 2007).

58 In addition to basic scientific research, the distribution and intensity of surface  
59 solar radiation is urgently needed for solar energy applications. All three components  
60 of solar radiation, i.e. global radiation, direct radiation and diffuse radiation, are



61 prerequisites for the siting, design, evaluation and optimization of different solar energy  
62 systems (Karakoti et al., 2011; Mellit et al., 2010). For example, photovoltaic (PV)  
63 power systems rely on global radiation to generate electricity, and global radiation on  
64 arbitrarily oriented PV panels can be calculated by direct and diffuse radiation, while  
65 concentrated solar power systems use only direct radiation to generate electricity  
66 (Boland et al., 2013; Tang et al., 2018). In addition, recently developed bifacial PV  
67 panels also use the backside of the PV panel to generate electricity, and the source of  
68 solar radiation on the backside is diffuse radiation (Rodríguez-Gallegos et al., 2018;  
69 Pelaez et al., 2019).

70 In-situ measurements are considered the most effective and direct means of  
71 obtaining surface solar radiation data. However, the number of radiation observation  
72 stations is very low due to high maintenance and calibration costs. For example,  
73 radiation fluxes measured at about 2500 stations worldwide are stored in the Global  
74 Energy Balance Archive (GEBA), a database that stores the different components of  
75 the surface energy budget from different data sources, such as national meteorological  
76 services, various experimental observation networks, and project reports (Wild et al.,  
77 2017). Among the GEBA, there are only about 100 radiation stations (Jiang et al. 2020a),  
78 which are provided by the China Meteorological Administration (CMA). Another issue  
79 is that the radiation observation stations are very unevenly distributed, with most of  
80 radiation stations being located in flat and densely populated areas, and with a very  
81 small number of stations being located in the complex terrain areas and sparsely  
82 populated areas. In addition, almost all radiation stations include global radiation



83 observations, but most of them do not include direct radiation and diffuse radiation  
84 observations. In addition, radiation measurements are considered to be more prone to  
85 problems and unreliable data than those of other meteorological variables. For example,  
86 erroneous or spurious data were frequently found in the CMA radiation observations  
87 (Shi et al., 2008; Tang et al., 2011). Therefore, the lack of long-term and dense solar  
88 radiation observations has become a tough challenge.

89         Satellites can provide continuous spatiotemporal observations, and retrieval based  
90 on satellite remote sensing is considered one of the most effective and commonly used  
91 means to fill the gap in ground-based radiation measurements (Lu et al., 2011; Zhang  
92 et al., 2014; Huang et al., 2019; Letu et al., 2021). In the past, satellite-based retrieval  
93 algorithms and corresponding radiation products have emerged, and the retrieval  
94 accuracy of the corresponding products has improved (Huang et al., 2019). In particular,  
95 retrievals applied to the new generation of geostationary satellites have improved in  
96 temporal resolution, spatial resolution and accuracy to varying degrees (Tang et al.,  
97 2019b; Letu et al., 2020). In general, the accuracy of the satellite-based radiation  
98 product is higher than that of the reanalysis product (Jiang et al., 2020b). Despite the  
99 obvious advantages, there are still several problems with satellite-based radiation  
100 products. First, the time series of satellite radiation products are generally not long  
101 enough to meet the demand for long time series data, such as for climate change studies.  
102 Second, the updating of satellite sensors and the fusion of multi-source satellites would  
103 lead to inconsistent data quality and introduce large uncertainties into the analysis of  
104 long-term variations (Feng and Wang, 2021a; Shao et al., 2022). Third, most satellite



105 radiation products only provide global radiation, but do not include direct and diffuse  
106 radiation, because the uncertainty in algorithms for estimating direct and diffuse  
107 radiation is much larger than the uncertainty in global radiation.

108       Alternatively, estimation based on meteorological variables observed at routine  
109 weather stations is another effective solution that can overcome the scarcity of radiation  
110 data, since the number of routine weather stations is much denser than that of radiation  
111 stations (Feng and Wang, 2021b). For example, there are only about 100 radiation  
112 stations maintained by CMA, but the number of routine weather stations with long-term  
113 observations is much denser, exceeding 2400 stations. Empirical models for estimating  
114 global radiation using surface meteorological variables were usually found in the  
115 hydrological and agricultural fields (Wang et al., 2016), and these models can be  
116 broadly classified into three types: air temperature-based models, sunshine-duration-  
117 based models, and cloud cover-based models (Liu et al., 2009; Ehnberg & Bollen, 2005).  
118 In general, a well-calibrated sunshine duration-based model was considered to perform  
119 better than the other two types of models (Pohlert, 2004). Although the above empirical  
120 models, especially the Ångström-Prescott relationships (Ångström, 1924; Prescott,  
121 1940), have been widely used and have achieved great success, these models require  
122 ground radiation observations for calibration and the calibrated parameters are usually  
123 site-dependent, which poses significant risks and challenges when applied in areas with  
124 sparse or no radiation observations.

125       Yang et al. (2001) developed a hybrid model to estimate daily global radiation by  
126 combining pure physical processes under clear skies and a parameterization formula



127 for cloud transmission under cloudy skies. The hybrid model has been shown to work  
128 well without local calibration (Yang et al., 2006; Yang et al., 2010). Tang et al. (2013)  
129 used this hybrid model to construct a dataset of daily global radiation at 716 CMA  
130 weather stations during 1961-2010, and also found that its accuracy was generally  
131 higher than that of locally calibrated empirical models and satellite-based retrievals.  
132 However, few studies have focused on the development of empirical models for direct  
133 and diffuse radiation estimates. Fortunately, Tang et al. (2018) also developed a similar  
134 hybrid model to estimate daily direct radiation by adopting the strategy of Yang et al.  
135 (2001) to estimate global radiation. Therefore, these two hybrid models provide us with  
136 an opportunity to construct daily surface solar radiation at routine weather stations, once  
137 the observations of meteorological variables are available. The constructed dataset will  
138 contribute to simulations of land surface processes, climate change analysis, and solar  
139 energy applications.

140 In this study, based on our previous study by Tang et al. (2013) for global radiation  
141 estimation, we expanded the number of stations, radiation elements and time length,  
142 and finally developed a dense station-based long-term and high-accuracy daily surface  
143 solar radiation dataset in China, including three elements of global radiation, direct  
144 radiation and diffuse radiation. The rest of the paper is organized as follows. The  
145 methods used to estimate daily global, direct and diffuse radiation at weather stations  
146 are presented in Section 2, and Section 3 describes the input data used to drive the  
147 station-based models, the in-situ data used to validate the accuracy of the developed  
148 dataset, and two satellite-based radiation products used for comparison with our



149 products. The performance of our dataset and two satellite-based radiation products  
150 against the in-situ data is evaluated in Section 4, and the information on data availability  
151 is described in Section 5. Finally, Section 6 presents the summary of this study.

152

## 153 2. Methods

154 In this study, daily global radiation and daily direct radiation were estimated using  
155 the hybrid model of Yang et al. (2006) and the method developed by Tang et al. (2018),  
156 respectively. Finally, daily diffuse radiation was calculated by subtracting direct  
157 radiation from global radiation. The methods for estimating daily global, direct and  
158 diffuse radiation can be simply described by the following five mathematical formulas:

$$159 \quad R_g = (R_{b,clr} + R_{d,clr})\tau_{c,g}, \quad (1)$$

$$160 \quad R_b = R_{b,clr}\tau_{c,dir}, \quad (2)$$

$$161 \quad R_d = R_g - R_b, \quad (3)$$

$$162 \quad \tau_{c,g} = 0.2505 + 1.1468 \left(\frac{n}{N}\right) - 0.3974 \left(\frac{n}{N}\right)^2, \quad (4)$$

$$163 \quad \tau_{c,dir} = 0.4868 \left(\frac{n}{N}\right) + 0.5132 \left(\frac{n}{N}\right)^2, \quad (5)$$

164 where  $R_g$ ,  $R_b$ , and  $R_d$  [ $\text{W m}^{-2}$ ] are the daily all-sky global, direct and diffuse radiation  
165 at the horizontal surface, respectively.  $R_{b,clr}$  and  $R_{b,clr}$  [ $\text{W m}^{-2}$ ] are the daily clear-sky  
166 global and direct radiation at the horizontal surface, respectively.  $\tau_{c,g}$  and  $\tau_{c,dir}$  are the  
167 cloud transmittance for the daily global and direct radiation, respectively.  $n$  and  $N$  are  
168 the actual sunshine duration and the maximum possible sunshine duration, respectively.  
169 The daily clear-sky global and direct radiation ( $R_{b,clr}$  and  $R_{b,clr}$ ) at the horizontal  
170 surface are calculated by the following equations:



$$171 \quad R_{b,clr} = \frac{1}{24\text{hours}} \int_{t1}^{t2} I_0 \bar{\tau}_b dt, \quad (6)$$

$$172 \quad R_{d,clr} = \frac{1}{24\text{hours}} \int_{t1}^{t2} I_0 \bar{\tau}_d dt, \quad (7)$$

$$173 \quad \bar{\tau}_b \approx \max(0, \bar{\tau}_o \bar{\tau}_w \bar{\tau}_g \bar{\tau}_r \bar{\tau}_a), \quad (8)$$

$$174 \quad \bar{\tau}_d \approx \max(0, 0.5 \bar{\tau}_o \bar{\tau}_w \bar{\tau}_g (1 - \bar{\tau}_r \bar{\tau}_a)), \quad (9)$$

$$175 \quad \bar{\tau}_o = \exp[-0.0365(ml)^{0.7136}], \quad (10)$$

$$176 \quad \bar{\tau}_g = \exp[-0.0117(m_c)^{0.3139}], \quad (11)$$

$$177 \quad \bar{\tau}_w = \min[1.0, 0.909 \ln(mw)], \quad (12)$$

$$178 \quad \bar{\tau}_r = \exp[-0.008735m_c(0.547 + 0.014m_c - 0.00038m_c^2 +$$
$$179 \quad 4.6 \times 10^{-6}m_c^3)^{-4.08}], \quad (13)$$

$$180 \quad \bar{\tau}_a = \exp\{-m\beta[0.6777 + 0.1464(m\beta) - 0.00626(m\beta)^2]^{-1.3}\}, \quad (14)$$

$$181 \quad m = 1/[\sin(h) + 0.15(57.296h + 3.885)^{-1.253}], \quad (15)$$

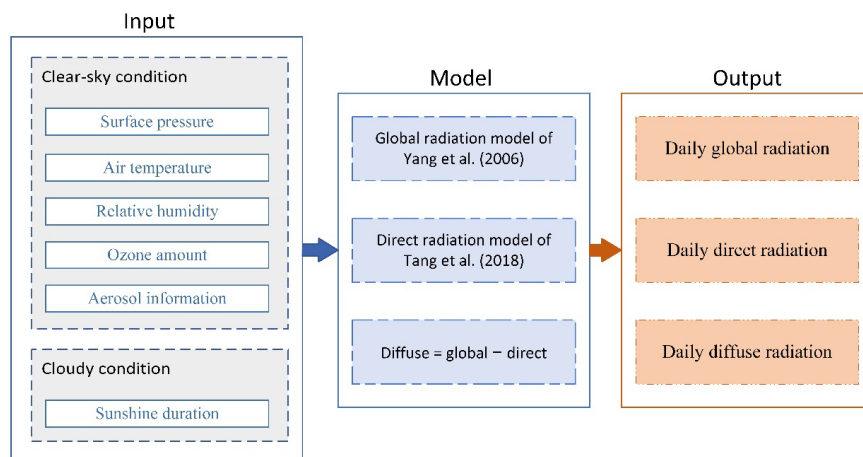
$$182 \quad m_c = mp_s/p_0, \quad (16)$$

183 where  $I_0$  [ $\text{W m}^{-2}$ ] is the horizontal solar radiation at the top of the atmosphere (TOA),  
184 and  $t1$  [hour] and  $t2$  [hour] are the times of sunrise and sunset, respectively.  $\bar{\tau}_b$  and  $\bar{\tau}_d$   
185 are the transmittances for the daily direct and diffuse radiation under clear skies,  
186 respectively.  $\bar{\tau}_o$ ,  $\bar{\tau}_g$ ,  $\bar{\tau}_w$ ,  $\bar{\tau}_r$ , and  $\bar{\tau}_a$  are transmittances due to ozone absorption,  
187 permanent gas absorption, water vapor absorption, Rayleigh scattering, and aerosol  
188 absorption and scattering in the atmospheric layer, respectively.  $m$  is the air mass, and  
189  $l$  (cm) is ozone layer thickness.  $m_c$  is the pressure-corrected air mass, and  $w$  (cm), is  
190 the precipitable water.  $\beta$  and  $h$  [radian] are the Ångström turbidity coefficient and the  
191 solar elevation angle, respectively.  $p_0$  [Pa] is the standard atmospheric pressure, and  $p_s$   
192 [Pa] is the surface pressure.



193 The overall flowchart for the estimation of the station-based radiation products is  
194 shown in Figure 1, which consists mainly of input, model and output sections. The  
195 inputs are surface pressure, air temperature, relative humidity, ozone amount, aerosol  
196 data and sunshine duration. Air temperature and relative humidity are used to estimate  
197 precipitable water. The aerosol Ångström turbidity is mainly converted from horizontal  
198 visibility observations measured at weather stations using the method of Tang et al.  
199 (2017a). The ozone amount is obtained from the zonal means of the Total Ozone  
200 Mapping Spectrometer (TOMS). The outputs are daily global, direct and diffuse  
201 radiation, respectively. For more detailed information on the above methods, we can  
202 refer to the articles by Yang et al. (2006) and Tang et al. (2018).

203



204

205 **Figure 1** Flowchart of data production, including input, model and output sections.

206

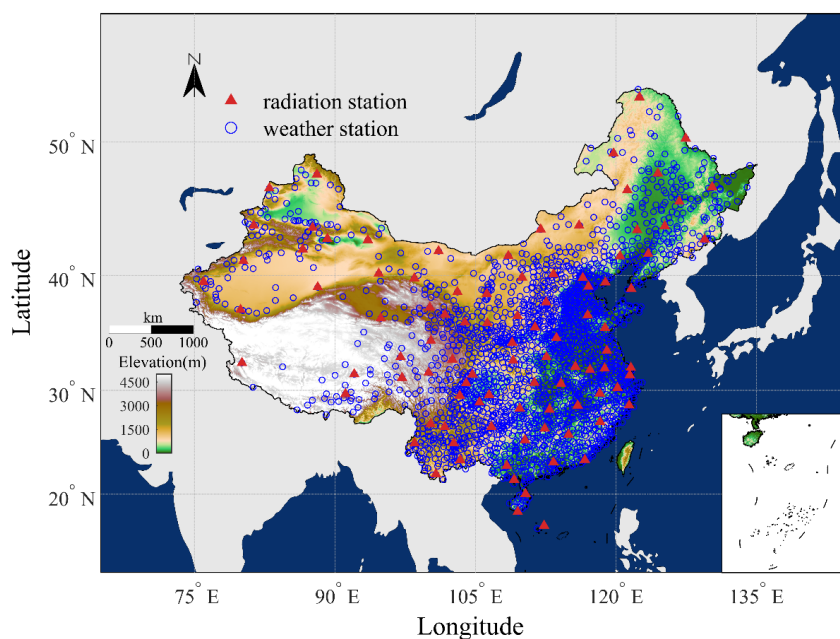
### 207 **3 Data**

#### 208 **3.1 Input data**



209 The inputs to the above methods for estimating daily global, direct and diffuse  
210 radiation are mainly surface pressure, air temperature, relative humidity, horizontal  
211 visibility, sunshine duration and ozone amount. With the exception of ozone, all input  
212 data are observed at the 2473 CMA routine meteorological stations, where the  
213 estimation methods can work well. Here, the ozone amount was used from the  
214 climatological data obtained from the TOMS zonal means. Figure 2 shows the spatial  
215 distribution of these routine meteorological stations, indicated by the small blue circles,  
216 with characteristics of a dense distribution in the eastern and southern regions of China  
217 and a sparse distribution in the western and northern regions of China.

218



219

220 **Figure 2** Spatial distribution of China Meteorological Administration weather station  
221 and radiation station. Red triangles represent radiation stations, and blue  
222 circles denote weather stations without radiation observation.



223 Finally, in this study, a dataset of more than 60 years of daily global, direct and  
224 diffuse radiation was constructed using the methods described above at the 2473 CMA  
225 routine meteorological stations from the 1950s to 2021, with most stations covering the  
226 period 1961-2021.

227

### 228 **3.2 In-situ radiation data**

229 Due to the extensive renewal and replacement of radiation instruments in 1993,  
230 and because more erroneous observations were found before 1993, radiation  
231 observations during the period 1993-2010 were used to evaluate the performance of our  
232 developed station-based radiation dataset and the other two satellite-based radiation  
233 products. Among the 2473 CMA routine meteorological stations, there are about 96  
234 radiation stations (denoted by the upper red triangle in Figure 2) where radiation  
235 observations have been carried out in addition to routine meteorological observations  
236 since 1993. Among the 96 CMA radiation stations, there are only 19 stations where  
237 direct and diffuse radiation observations are carried out in addition to global radiation  
238 observations.

239 One issue to note is that we did not use the direct radiation observations as  
240 validation basis, but the value obtained by subtracting the diffuse radiation observations  
241 from the global radiation observations, because the quality of the direct radiation  
242 observations is significantly lower than that of the global and diffuse radiation  
243 observations (Tang et al., 2018). Another issue that we need to be aware of is that  
244 obviously erroneous or false values have usually been found in the CMA radiation data



245 (Shi et al., 2008), although a preliminary quality check of the raw radiation observations  
246 was carried out before release. Therefore, we further applied the quality control  
247 procedures developed by Tang et al. (2010) to the raw radiation observations and  
248 filtered out the corresponding spurious and erroneous observations. More detailed  
249 information on the quality control scheme can be found in the article by Tang et al.  
250 (2010).

251

### 252 **3.3 Satellite-based radiation products**

253 In this study, two satellite-based radiation products (Jiang et al., 2020a; Tang et  
254 al., 2019a) were used for comparison with our station-based radiation dataset estimated  
255 at 2743 CMA routine meteorological stations.

256 One is the product of Jiang et al. (2020a), which provides hourly global radiation  
257 and diffuse radiation in China with a spatial resolution of ~5 km and a time span from  
258 2007 to 2018. The product was generated using a deep learning algorithm developed  
259 by Jiang et al. (2019) to retrieve global radiation, and a transfer learning approach to  
260 retrieve diffuse radiation from Multi-functional Transport Satellites (MTSAT) imagery.  
261 The algorithm successfully tackled spatial adjacency effects induced by photon  
262 transport through convolutional neural networks, resulting in excellent performance in  
263 instantaneous radiation retrieval, especially for diffuse radiation (Jiang et al., 2020c).

264 The other is the high-resolution global product of global radiation developed by  
265 Tang et al. (2019a) based on the latest cloud products of the International Satellite  
266 Cloud Climatology Project H-series pixel-level global (ISCCP-HXG), routine



267 meteorological variables of the ERA5 reanalysis data, aerosol optical thickness of the  
268 MERRA-2 reanalysis data, and albedo of the MODIS and CM-SAF products with the  
269 physical algorithm of Tang et al. (2017b). This global product has a spatial resolution  
270 of 10 km, a temporal resolution of 3 hours, and spans the period 1983.7-2018.12. Global  
271 comparative validation with observations shows that the accuracy of this global  
272 radiation product is generally better than several global satellite radiation products, such  
273 as the Earth's Radiant Energy System (CERES; Kato et al., 2013), the Global Energy  
274 and Water Cycle Experiment surface radiation budget (GEWEX-SRB; Pinker and  
275 Laszlo, 1992), and the ISCCP flux dataset (ISCCP-FD; Zhang et al., 2004).

276 In this study, these two satellite-based radiation products were first averaged to  
277 daily and monthly means, and then validated against observations collected at the CMA  
278 radiation stations, and finally compared with our station-based radiation dataset in  
279 China.

280

#### 281 **4 Results and Discussion**

282 The station-based radiation dataset was first validated against the CMA radiation  
283 observations at daily and monthly scales, respectively, then compared with two other  
284 satellite-based radiation products, and finally its spatial distribution characteristics were  
285 further analyzed. These are described in detail in the following four subsections. In this  
286 study, we used the statistical metrics of mean bias error (MBE), relative MBE (rMBE),  
287 root mean square error (RMSE), relative RMSE (rRMSE) and correlation coefficient  
288 (R) to measure the accuracies of our station-based dataset and the other two satellite-



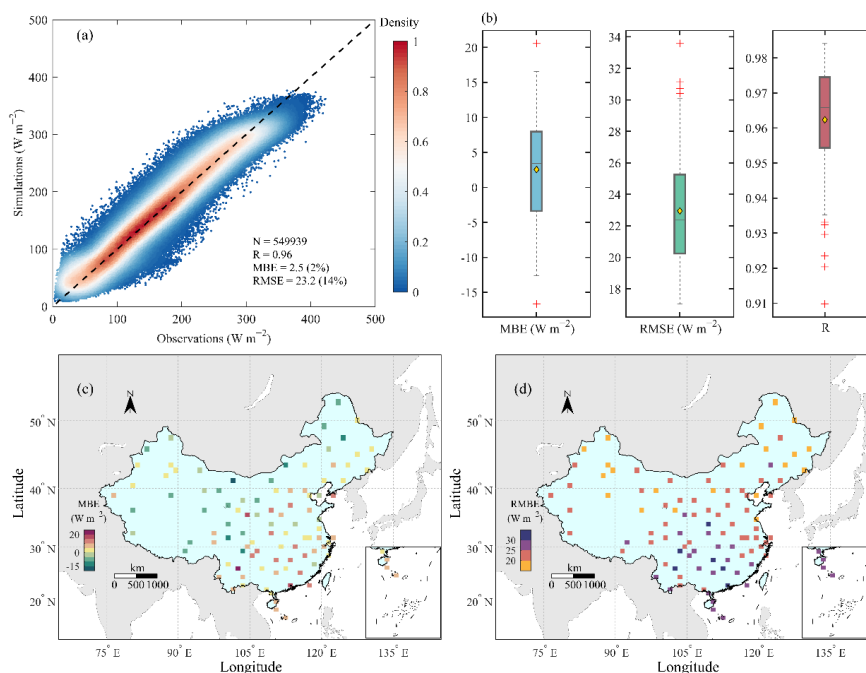
289 based radiation products.

290

#### 291 **4.1 Validation at daily scale**

292 Figure 3 shows the validation results for the daily global radiation estimates  
293 against observations from 96 CMA radiation stations over the period of 1993-2010.  
294 Overall, our station-based estimates over China perform well, with an MBE of 2.5 W  
295  $\text{m}^{-2}$ , a RMSE of 23.2  $\text{W m}^{-2}$ , and an R of 0.96 (Figure 3 a). This indicates that the  
296 accuracy of our station-based estimates is significantly higher than that of almost all of  
297 the satellite products (such as, ISCCP-FD, GEWEX-SRB, CERES, GLASS and  
298 ISCCP-HXG) and reanalysis data (such as, ERA5 and MERRA-2), as well as other  
299 regional satellite-based radiation products from Tang et al. (2016), Jiang et al. (2020a),  
300 and Letu et al. (2021). In terms of MBE, there is a slight positive deviation, but the  
301 relative deviation is close to 2%, which is within the tolerance range of the PV potential  
302 assessment.

303 In addition, we also calculated the statistical metrics for each radiation station and  
304 their boxplots and spatial distributions are shown in Figure 3 (b)-(d). It can be seen that  
305 most of the stations had MBE between  $-4$  and  $8 \text{ W m}^{-2}$ , RMSE less than  $25 \text{ W m}^{-2}$ , and  
306 R greater than 0.95. The stations with relatively large errors were mainly found in the  
307 southern and eastern regions of China. This is largely due to the fact that these regions  
308 have more cloud cover and overcast skies, making it difficult to use sunshine duration  
309 to accurately parameterize cloud transmission. In addition, the uncertainty in the aerosol  
310 data would also partly contribute to the large errors.



311

312 **Figure 3** Validation results for our station-based daily global radiation dataset against

313 observations collected at 96 CMA radiation stations during 1993-2010. (a)

314 Comparison of daily global radiation between our dataset and observations,

315 (b) Boxplots of three statistical error metrics (MBE, RMSE and R), (c) spatial

316 distribution of MBE for individual radiation station, and (d) spatial

317 distribution of RMSE for individual radiation station.

318

319 Similar evaluations for the daily direct and diffuse radiation estimates are

320 presented in Figure 4 and Figure 5, respectively. Averaged over 19 CMA radiation

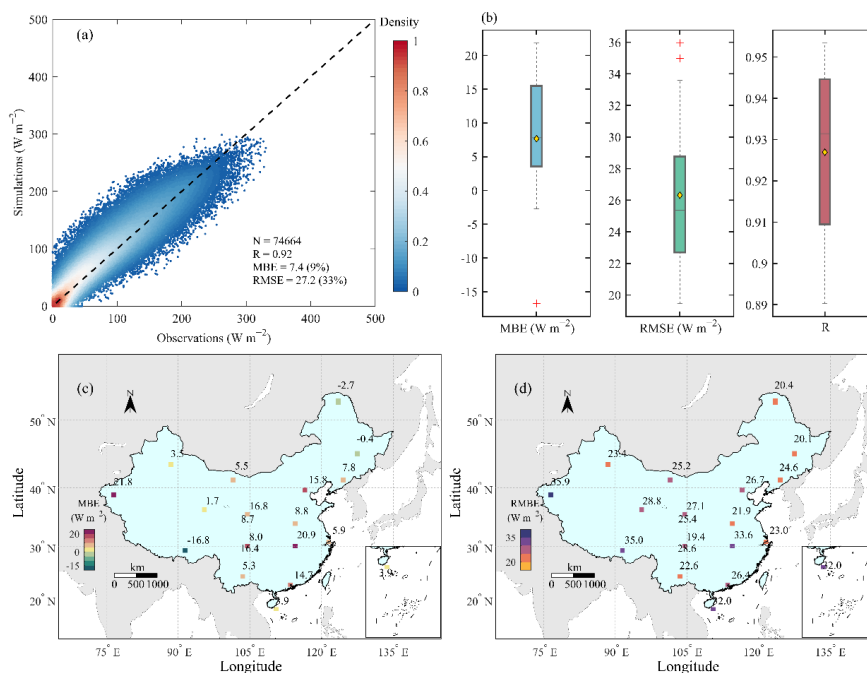
321 stations, our estimates for daily direct radiation produces an MBE of  $7.4 \text{ W m}^{-2}$ , a

322 RMSE of  $27.2 \text{ W m}^{-2}$  and an R of 0.92, respectively; while our estimates for daily

323 diffuse radiation produces an MBE of  $-3.3 \text{ W m}^{-2}$ , a RMSE of  $19.2 \text{ W m}^{-2}$  and a R of



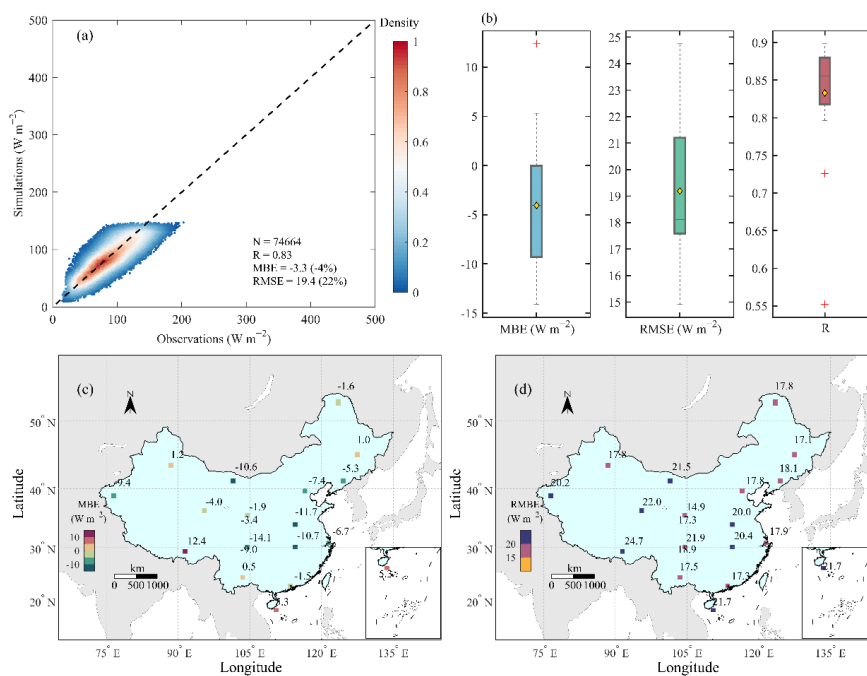
324 0.83, respectively. Both accuracies for direct and diffuse radiation are lower than for  
325 global radiation, as can be seen from their rRMSE and rMBE. The absolute rMBE for  
326 global radiation is about 2%, while those for direct and diffuse radiation are about 9%  
327 and 4%, respectively. The rRMSE for global radiation is about 14%, while those for  
328 direct and diffuse radiation are about 33% and 22%, respectively. We found that there  
329 is a slight overestimation for direct radiation, with an MBE of about  $7.4 \text{ W m}^{-2}$ . This  
330 may be due to the presence of high clouds, in which case the cloud transmission for  
331 direct radiation cannot be well parameterized by the sunshine duration (Tang et al.  
332 2018). For direct radiation, the RMSE at most stations is less than  $29 \text{ W m}^{-2}$  and the R  
333 at most stations is greater than 0.91; for diffuse radiation, the RMSE at most stations is  
334 less than  $21 \text{ W m}^{-2}$  and the R at most stations is greater than 0.81. The largest RMSE  
335 for both direct and diffuse radiation is found at the Lhasa station, where popcorn clouds  
336 were common, posing a major challenge to the simulation of cloud transmittance with  
337 sunshine duration.



338

339

Figure 4 Same as Figure 3, but for daily direct radiation.



340

341

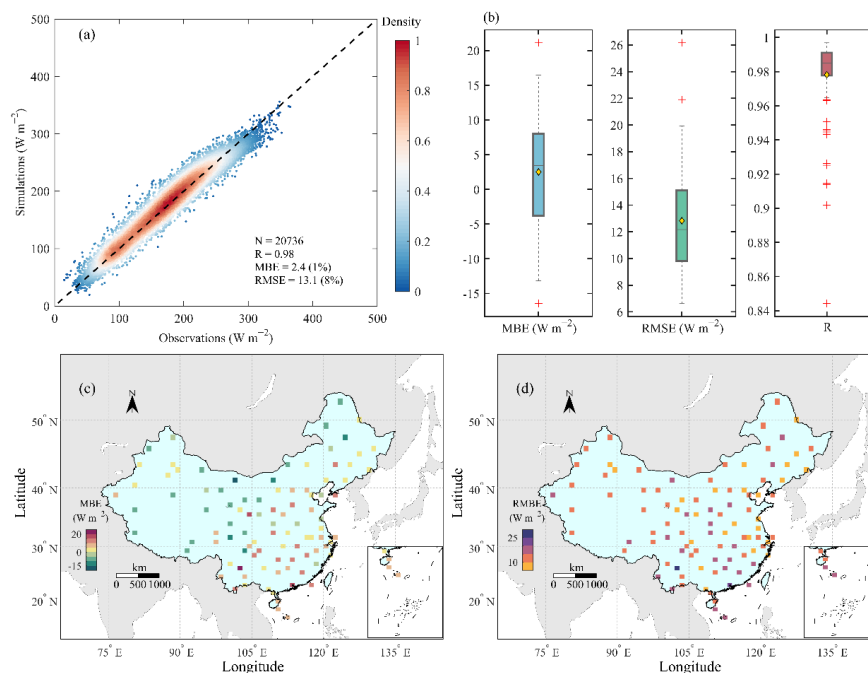
Figure 5 Same as Figure 3, but for daily diffuse radiation.



342 **4.2 Validation at monthly scale**

343 Based on the daily estimates, we also calculated their monthly averages and  
344 validated them against observations. Figure 6 shows the validations for the estimates of  
345 monthly global radiation against observations at the CMA radiation stations. Averaged  
346 over all stations, the monthly global radiation estimates give an MBE of  $2.4 \text{ W m}^{-2}$ , a  
347 RMSE of  $13.1 \text{ W m}^{-2}$  and an R of 0.98. The rRMSE is about 8%. From the boxplots of  
348 the error indicators, R was greater than 0.98 and RMSE was less than  $15 \text{ W m}^{-2}$  at most  
349 stations. The spatial distribution features of MBE and RMSE are similar to those for  
350 daily global radiation, with relatively larger errors in the southern and eastern regions  
351 of China, and the largest MBE and RMSE are both found at Panzhihua station (with  
352 longitude of  $101.717^\circ$  and latitude of  $26.583^\circ$ ).

353



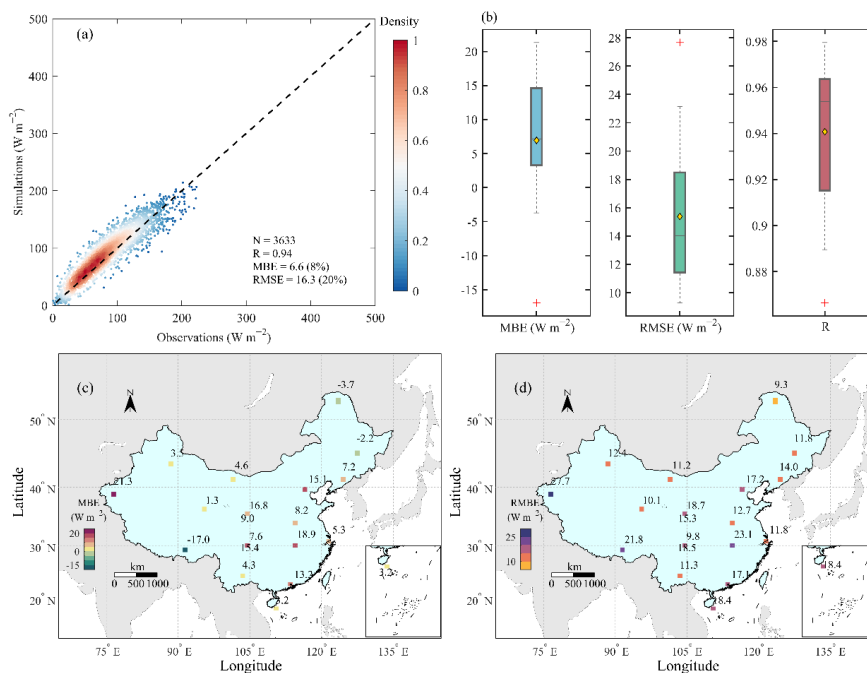
354



355                    **Figure 6** Same as **Figure 3**, but for monthly global radiation.

356

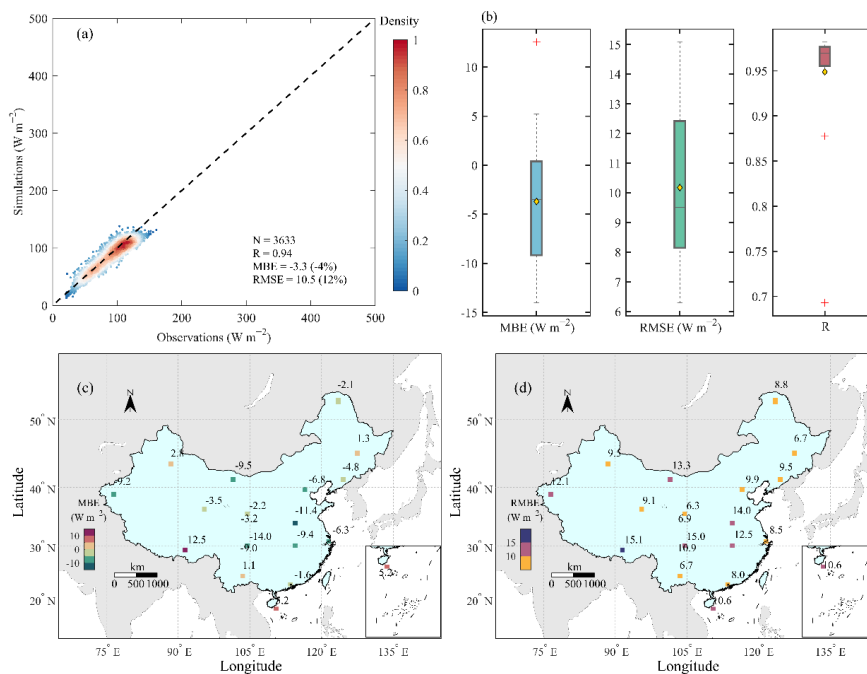
357                    Figure 7 and Figure 8 also show the validation results for monthly direct and  
358 diffuse radiation against 19 CMA radiation stations. The rRMSE values for monthly  
359 direct and global radiation are 20% and 12%, respectively. The MBE, RMSE and R for  
360 monthly direct radiation are  $6.6 \text{ W m}^{-2}$ ,  $16.3 \text{ W m}^{-2}$  and 0.94, respectively, while the  
361 MBE, RMSE and R for monthly diffuse radiation are  $-3.3 \text{ W m}^{-2}$ ,  $10.5 \text{ W m}^{-2}$  and 0.94,  
362 respectively. Similar to the case of the daily scale, a slight overestimation is also found  
363 for the monthly direct radiation. The RMSE for monthly direct and diffuse radiation is  
364 less than  $18 \text{ W m}^{-2}$  and  $13 \text{ W m}^{-2}$ , respectively, at most stations, while R for monthly  
365 direct and diffuse radiation is greater than 0.91 and 0.95, respectively, at most stations.  
366 The spatial distribution characteristics of MBE and RMSE are similar to those of daily  
367 conditions for both direct and diffuse radiation.



368

369

**Figure 7** Same as **Figure 3**, but for monthly direct radiation.



370

371

**Figure 8** Same as **Figure 3**, but for monthly diffuse radiation.



### 372 **4.3 Comparison with satellite-based products**

373 To demonstrate the superiority of the station-based radiation dataset developed in  
374 this study, we compared the station-based dataset with two widely used satellite-based  
375 radiation products. One is the product developed with deep learning and trained with  
376 surface radiation observations (Jiang et al., 2020a), and the other is the long-term global  
377 product of global radiation (Tang et al., 2019a), which was mainly developed based on  
378 the latest ISCCP-HXG cloud products with the improved physical algorithm (Tang et  
379 al., 2017b). The former can provide hourly global, direct and diffuse radiation, while  
380 the latter can only provide the 3-hourly global radiation. Here, we use a  $3 \times 3$  spatial  
381 window to smooth the raw radiation product from Tang et al. (2019a), as its accuracy  
382 is clearly improved when upscaled to 30 km. As we only have access to the CMA  
383 radiation observations up to 2010, the time period chosen for comparison is 2000-2010.  
384 Table 1 and Table 2 present the comparison of the evaluation results among the three  
385 radiation products against the observations measured at all CMA radiation stations from  
386 2000 to 2010, for daily and monthly conditions, respectively.

387 For daily data comparisons, our station-based estimate for daily global radiation  
388 obviously outperforms the other two satellite-based radiation products, with MBE of  
389  $2.7 \text{ W m}^{-2}$ , RMSE of  $23.2 \text{ W m}^{-2}$  and R of 0.96, followed by the product of Tang et al.  
390 (2019a) (with MBE of  $6.7 \text{ W m}^{-2}$ , RMSE of  $26.8 \text{ W m}^{-2}$  and R of 0.95) and the product  
391 of Jiang et al. (2020a) (with MBE of  $4.4 \text{ W m}^{-2}$ , RMSE of  $33.6 \text{ W m}^{-2}$  and R of 0.92).  
392 Our station-based estimates for daily direct radiation are also apparently more accurate  
393 than the satellite-based product of Jiang et al. (2020a), with the former producing a



394 lower RMSE and a higher R. The RMSE of our estimates is about 9 W m<sup>-2</sup> lower than  
395 that of the product of Jiang et al. (2020a).

396 For the daily diffuse radiation, our estimate is comparable to the diffuse radiation  
397 product of Jiang et al. (2020a)'s. It should be noted that the CMA radiation observations  
398 were used to train the deep learning model of Jiang et al. (2020a), while no observations  
399 were used in our estimates. Overall, these results indicate that the station-based  
400 estimates of global, direct and diffuse radiation generally outperform those from  
401 satellite retrievals.

402

403 **Table 1.** Accuracy comparisons of our estimates in this study with other two satellite-  
404 based products at daily scale. The units of MBE and RMSE are both W m<sup>-2</sup>.  
405 Observations of global radiation measured at 96 CMA radiation stations, and  
406 observations of direct radiation and diffuse radiation measured at 19 CMA radiation  
407 stations during 2000-2010 are used.

	This study			Jiang et al. (2020a)			Tang et al. (2019a)
	global	direct	diffuse	global	direct	diffuse	global (30 km)
MBE	2.7	8.6	-3.8	4.4	8.6	0.1	6.7
RMSE	23.2	27.6	19.6	33.6	36.6	20.1	26.8
R	0.96	0.92	0.83	0.92	0.85	0.84	0.95
N	328977	43630	43630	328977	43630	43630	328977

408

409 For the monthly comparisons, we also found that our estimate of monthly global



410 radiation is clearly more accurate than the two satellite products. The MBE and RMSE  
 411 of our estimate are  $2.6 \text{ W m}^{-2}$  and  $13.4 \text{ W m}^{-2}$ , respectively, which are lower than those  
 412 of the two satellite products, which are  $4.6 \text{ W m}^{-2}$  and  $18.5 \text{ W m}^{-2}$  for the Jiang et al.  
 413 (2020a) product and  $6.7 \text{ W m}^{-2}$  and  $16.3 \text{ W m}^{-2}$  for the Tang et al. (2019a) product. The  
 414 R of our estimate is 0.98, which is higher than that of the two satellite products. Our  
 415 direct radiation estimate also outperforms the satellite product of Jiang et al. (2020a),  
 416 with the former having lower RMSE and MBE and higher R. Similar to the daily  
 417 comparison, the two monthly diffuse products are comparable to each other.

418

419 **Table 2.** Accuracy comparisons of our estimates in this study with other two satellite-  
 420 based products at monthly scale. The units of MBE and RMSE are both  $\text{W m}^{-2}$ .  
 421 Observations of global radiation measured at 96 CMA radiation stations, and  
 422 observations of direct radiation and diffuse radiation measured at 19 CMA radiation  
 423 stations during 2000-2010 are used.

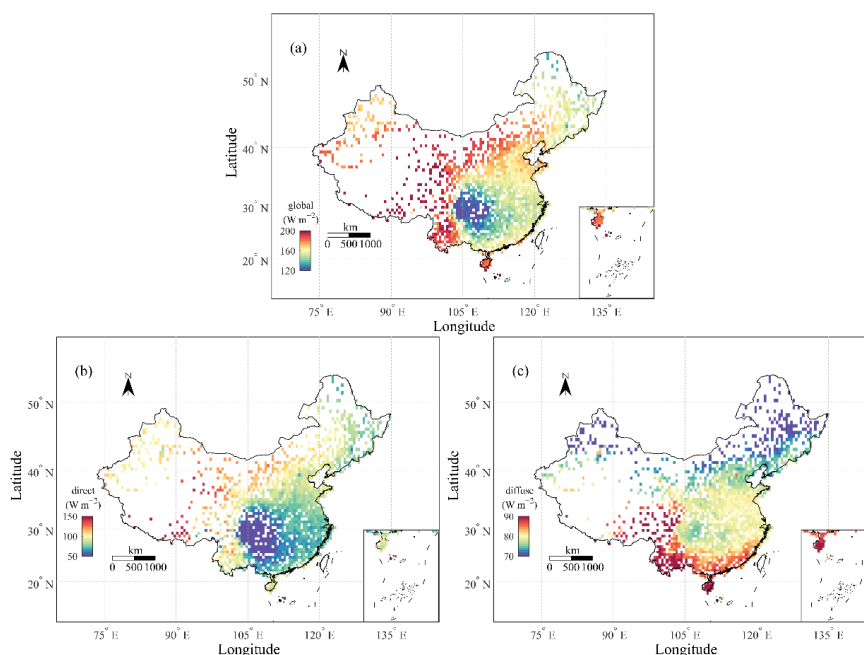
	This study			Jiang et al. (2020a)			Tang et al. (2019a)
	global	direct	diffuse	global	direct	diffuse	global (30 km)
MBE	2.6	7.9	-3.7	4.6	9.0	-0.5	6.7
RMSE	13.4	16.5	10.9	18.5	21.3	12.1	16.3
R	0.98	0.94	0.94	0.96	0.89	0.93	0.97
N	12059	2088	2088	12059	2088	2088	12059

424

#### 425 4.4 Spatial distribution features of solar radiation in China



426           Based on the developed station-based solar radiation dataset, Figure 8 present the  
427   spatial distributions of the multi-year average global, direct and diffuse radiation in  
428   China during 1961 -2021. The spatial distribution of direct radiation is similar to that  
429   of global radiation, with the highest value over the Tibetan Plateau and the lowest value  
430   over the Sichuan Basin. However, the spatial distribution of diffuse radiation is very  
431   different from that of global radiation, with the highest value being found at the  
432   southernmost tip of China, and the lowest value being found in northeastern China. In  
433   general, clear-sky days correspond to more direct radiation and cloudy days correspond  
434   to more diffuse radiation, mainly because the scattering effect of aerosols is much  
435   smaller than the scattering effect of clouds. Therefore, high direct radiation is usually  
436   found in areas with frequent sunny days, such as Northwest China, North China and  
437   Inner Mongolia, while low direct radiation is usually found in areas with frequent cloud  
438   cover, such as East China and South China. The opposite is true for diffuse radiation.  
439



440

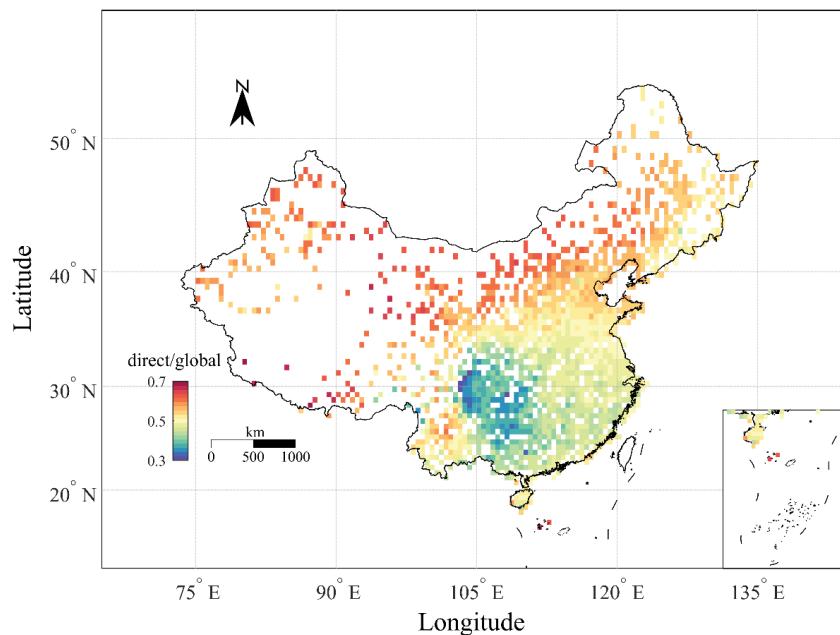
441 **Figure 9** Spatial distribution of the multi-year mean (a) global radiation, (b) direct  
442 radiation, and (c) diffuse radiation from the station-based radiation dataset in  
443 China during 1961-2021.

444

445 The spatial distribution of the multi-year average ratio of direct radiation to global  
446 radiation in China during the period of 1961-2021 is also shown in Figure 10. Direct  
447 radiation is mainly greater than diffuse radiation (ratio < 50%) in northern China,  
448 northeastern China, northwestern China and the Tibetan Plateau, while diffuse radiation  
449 dominates in eastern and southern China. This information can guide the planning of  
450 solar PV power and concentrating solar power (CSP) in China. For example, regions  
451 such as Xinjiang, Inner Mongolia, Gansu and the Tibetan Plateau with a high proportion  
452 of direct radiation are suitable for the construction of CSP projects. Regions such as



453 Hainan, Yunnan, Guangxi and Guangdong with relatively high global and diffuse  
454 radiation are suitable for the use of bifacial PV panels, as both sides of the panels can  
455 be used to generate electricity and the main source on the back is from diffuse radiation.  
456 Conversely, in areas with low diffuse radiation, it may not be necessary to use bifacial  
457 PV panels.  
458



459  
460 **Figure 10** Spatial distribution of the multi-year mean ratio of direct radiation to global  
461 radiation from the station-based radiation dataset in China during 1961-  
462 2021.

## 463 464 **5 Data availability**

465 The dense station-based long-term dataset of daily global, direct and diffuse  
466 radiation product with high-accuracy is stored at the National Tibetan Plateau Data



467 Center (<https://data.tpc.ac.cn/en/disallow/55fc9768-ea6a-4d16-9207-28f6aed4900b>  
468 and <https://doi.org/10.11888/Atmos.tpc.300461>, Tang, 2023), Institute of Tibetan  
469 Plateau Research, Chinese Academy of Sciences.

470

## 471 **6 Summary**

472 In this study, we have developed a dense station-based long-term dataset of daily  
473 surface solar radiation in China with high-accuracy. The dataset consists of estimates  
474 of three radiation components (global, direct and diffuse radiation) at the 2473 CMA  
475 meteorological stations during the period from the 1950s to 2021, with most stations  
476 covering the period of 1961-2021. The methods used to develop the dataset are the  
477 global radiation estimation model of Yang et al. (2006) and the direct radiation  
478 estimation model of Tang et al. (2018), and the main inputs are the five meteorological  
479 variables of surface pressure, air temperature, relative humidity, horizontal visibility,  
480 and sunshine duration measured at the meteorological stations. The developed dataset  
481 was evaluated against in-situ measurement collected at 96 CMA radiation stations, and  
482 further compared with other two satellite-based radiation products.

483 Averaged over all radiation stations and the time period of 1993-2010, the total  
484 RMSE values for daily global, direct and diffuse radiation are 23.2, 27.6 and 19.6 W  
485 m<sup>-2</sup>, respectively. At the monthly mean scale, our estimates give RMSE values of about  
486 13.4, 16.5 and 10.9 W m<sup>-2</sup>, respectively, for monthly global, direct and diffuse radiation.  
487 These error indicators on both daily and monthly scales are generally lower than those  
488 of the satellite radiation products, especially for global and direct radiation.



489 Comparisons with the satellite-based radiation products indicate that our station-based  
490 estimates have a clear advantage in terms of accuracy and length of time series.  
491 However, our dataset does not provide radiation data beyond the weather stations.  
492 Merging the station-based estimates with the satellite-based retrievals will have good  
493 potential to improve the accuracy of the radiation products in the future. We expect that  
494 our station-based radiation dataset to contribute significantly to relevant basic research,  
495 engineering applications and fusion with satellite-based retrievals in the future.

496

497 **Author contributions.** All authors discussed the results and contributed to the  
498 manuscript. WT calculated the dataset, analyzed the results, and drafted the manuscript.  
499 JH drew the figures.

500

501 **Competing interests.** The authors declare that they have no conflicts of interest.

502

503 **Acknowledgments.** The ISCCP-HXG global product of global radiation was provided  
504 by the National Tibetan Plateau Data Center (TPDC). The radiation product of Jiang et  
505 al. (2016) was available from the Pangaea at  
506 <https://doi.org/10.1594/PANGAEA.904136>, and the CMA routine meteorological  
507 variables and radiation data were obtained from the CMA Meteorological Information  
508 Center. The authors would like to thank the staff of the data management and production  
509 organizations for their valuable work.

510



511 **Financial support.** This work was supported by the National Key Research and  
512 Development Program of China (Grant No. 2022YFB4202104), and the National  
513 Natural Science Foundation of China (Grant No. 42171360).

514

#### 515 **References**

516 Alton, P. B., North, P. R., Los, S. O.: The impact of diffuse sunlight on canopy light-  
517 use efficiency, gross photosynthetic product and net ecosystem exchange in three  
518 forest biomes. *Global Change Biology*, 13: 776-787, 2007.

519 Ångström, A.: Solar and terrestrial radiation. *Q.J.R. Meteorol. Soc.*50, 121-125, 1924.

520 Boland, J., Huang, J., & Ridley, B.: Decomposing global solar radiation into its direct  
521 and diffuse components. *Renewable and Sustainable Energy Reviews*, 28, 749-  
522 756. <https://doi.org/https://doi.org/10.1016/j.rser.2013.08.023>, 2013.

523 Ehnberg, J. S. G., & Bollen, M. H. J.: Simulation of global solar radiation based on  
524 cloud observations. *Solar Energy*, 78(2), 157–162.  
525 <https://doi.org/10.1016/j.solener.2004.08.016>, 2005.

526 Feng, F., Wang, K.: Merging high-resolution satellite surface radiation data with  
527 meteorological sunshine duration observations over China from 1983 to 2017.  
528 *Remote Sensing*. 13(4), 602, 2021a.

529 Feng, F., and Wang, K.: Merging ground-based sunshine duration observations with  
530 satellite cloud and aerosol retrievals to produce high-resolution long-term surface  
531 solar radiation over China, *Earth System Science Data*, 13(3): 907-922, 2021b.

532 Gu, L. H., Baldocchi, D., Verma, S. B., et al.: Advantages of diffuse radiation for



- 533 terrestrial ecosystem productivity. *Journal of Geophysical Research-Atmospheres*,  
534 107: 4050, 2002.
- 535 Huang, G., Li, Z., Li, X., Liang, S., Yang, K., Wang, D., and Zhang, Y.: Estimating  
536 surface solar irradiance from satellites: Past, present, and future perspectives,  
537 *Remote Sens. Environ.*, 233, 111371, <https://doi.org/10.1016/j.rse.2019.111371>,  
538 2019.
- 539 Jiang, H., Lu, N., Qin, J., Tang, W. & Yao, L.: A deep learning algorithm to estimate  
540 hourly global solar radiation from geostationary satellite data. *Renewable &  
541 Sustainable Energy Reviews*, 114, 109327, 2019.
- 542 Jiang, H., Lu, N., Qin, J., & Yao, L.: Hourly 5-km surface total and diffuse solar  
543 radiation in China, 2007–2018. *Scientific Data*, 7(1).  
544 <https://doi.org/10.1038/s41597-020-00654-4>, 2020a.
- 545 Jiang, H., Yang, Y., Bai, Y. & Wang, H.: Evaluation of the total, direct, and diffuse solar  
546 radiations from the ERA5 reanalysis data in China. *IEEE Geosci. Remote S.* 17,  
547 47–51, 2020b.
- 548 Jiang, H., Yang, Y., Wang, H., Bai, Y. & Bai, Y.: Surface diffuse solar radiation  
549 determined by reanalysis and satellite over East Asia: evaluation and comparison.  
550 *Remote Sensing*, 12, 1387, 2020c.
- 551 Karakoti, I., Pande, B., & Pandey, K.: Evaluation of different diffuse radiation models  
552 for Indian stations and predicting the best fit model. *Renewable and Sustainable  
553 Energy Reviews*, 15(5), 2378-2384.  
554 <https://doi.org/https://doi.org/10.1016/j.rser.2011.02.020>, 2011.



- 555 Kato, S., Loeb, N. G., Rose, F. G., Doelling, D. R., Rutan, D. A., Caldwell, T. E., Yu,  
556 L., and Weller, R. A.: Surface irradiances consistent with CERES-derived top-of-  
557 atmosphere shortwave and longwave irradiances, *J. Climate*, 26, 2719–2740, 2013.
- 558 Lee, M. et al.: Model-based analysis of the impact of diffuse radiation on CO<sub>2</sub> exchange  
559 in a temperate deciduous forest. *Agr. Forest Meteorol.* 249, 377–389, 2017.
- 560 Letu, H., Yang, K., Nakajima, T. Y., Ishimoto, H., Nagao, T. M., Riedi, J., Baran, A. J.,  
561 Ma, R., Wang, T., Shang, H., Khatri, P., Chen, L., Shi, C., Shi, J.: High-resolution  
562 retrieval of cloud microphysical properties and surface solar radiation using  
563 Himawari-8/AHI next-generation geostationary satellite. *Remote Sens. Environ.*,  
564 239, 111583, <http://dx.doi.org/10.1016/j.rse.2019.111583>, 2020.
- 565 Letu, H., Nakajima, T.Y., Wang, T.X., Shang, H.Z., Ma, R., Yang, K., Baran, A.J., Riedi,  
566 J., Ishimoto, H., Yoshida, M., Shi, C., Khatri, P., Du, Y.H., Chen, L.F., & Shi, J.C.:  
567 A new benchmark for surface radiation products over the East Asia-Pacific region  
568 retrieved from the Himawari-8/AHI next-generation geostationary satellite.  
569 *Bulletin of the American Meteorological Society*, 2021, E873–E888,  
570 <https://journals.ametsoc.org/view/journals/bams/103/3/BAMS-D-20-0148.1.xml>,  
571 2021.
- 572 Liu, X. Y., Mei, X. R., Li, Y. Z., Wang, Q., Jensen, J. R., Zhang, Y., & Porter, J. R.:  
573 Evaluation of temperature-based global solar radiation models in China.  
574 *Agricultural and Forest Meteorology*, 149, 1433–1446, 2009.
- 575 Lu, N., Qin, J., Yang, K., and Sun, J.: A simple and efficient algorithm to estimate daily  
576 global solar radiation from geostationary satellite data, *Energy*, 36, 3179–3188,



- 577 <https://doi.org/10.1016/j.energy.2011.03.007>, 2011.
- 578 Mellit, A., Eleuch, H., Benghanem, M., Elaoun, C., & Pavan, A. M.: An adaptive model  
579 for predicting of global, direct and diffuse hourly solar irradiance. Energy  
580 Conversion and Management, 51(4), 771-782.  
581 <https://doi.org/https://doi.org/10.1016/j.enconman.2009.10.034>, 2010.
- 582 Mercado L. M., Bellouin N., Sitch S., et al.: Impact of changes in diffuse radiation on  
583 the global land carbon sink. Nature, 458: 1014-1017, 2009.
- 584 Pelaez, S. A., Deline, C., Macalpine, S. M., Marion, B., Stein, J. S., & Kostuk, R. K.:  
585 Comparison of Bifacial Solar Irradiance Model Predictions With Field Validation.  
586 IEEE Journal of Photovoltaics, 9(1), 82-88.  
587 <https://doi.org/10.1109/jphotov.2018.2877000>, 2019.
- 588 Pinker, R. T. and Laszlo, I.: Modeling surface solar irradiance for satellite application  
589 on a global scale, J. Appl. Meteorol., 31, 194–211, [https://doi.org/10.1175/1520-0450\(1992\)031<0194:MSSIFS>2.0.CO;2](https://doi.org/10.1175/1520-0450(1992)031<0194:MSSIFS>2.0.CO;2), 1992.
- 591 Pohlert, T.: Use of empirical global radiation models for maize growth simulation.  
592 Agric. Forest Meteorol. 126, 47–58, 2004.
- 593 Prescott, J.A.: Evaporation from a water surface in relation to solar radiation. Trans.  
594 Roy. Soc. Austr. 641, 114-125, 1940.
- 595 Rodríguez-Gallegos, C. D., Bieri, M., Gandhi, O., Singh, J. P., Reindl, T., & Panda, S.  
596 K.: Monofacial vs bifacial Si-based PV modules: Which one is more cost-effective?  
597 Solar Energy, 176, 412-438.  
598 <https://doi.org/https://doi.org/10.1016/j.solener.2018.10.012>, 2018.



- 599 Shao, C., Yang, K., Tang, W., et al.: Convolutional neural network-based  
600 homogenization for constructing a long-term global surface solar radiation dataset.  
601 Renewable and Sustainable Energy Reviews. 169, 112952, 2022.
- 602 Shi, G.Y., Hayasaka, T., Ohmura, A., Chen, Z.H., Wang, B., Zhao, J.Q., Che, H.Z., Xu,  
603 L.: Data quality assessment and the long-term trend of ground solar radiation in  
604 China. J. Appl. Meteor. Climatology, 47, 1006–1016, 2008.
- 605 Tang, W., Yang, K., He, J., & Qin, J.: Quality control and estimation of global solar  
606 radiation in China. Solar Energy, 84(3), 466–475.  
607 <https://doi.org/10.1016/j.solener.2010.01.006>, 2010.
- 608 Tang, W. J., Yang, K., Qin, J., Cheng, C. C. K., & He, J.: Solar radiation trend across  
609 China in recent decades: a revisit with quality-controlled data. Atmospheric  
610 Chemistry and Physics, 11(1), 393–406. <https://doi.org/10.5194/acp-11-393-2011>,  
611 2011.
- 612 Tang, W., Yang, K., Qin, J., & Min, M.: Development of a 50-year daily surface solar  
613 radiation dataset over China. Science China Earth Sciences, 56(9), 1555–1565.  
614 <https://doi.org/10.1007/s11430-012-4542-9>, 2013.
- 615 Tang, W., Qin, J., Yang, K., Liu, S., Lu, N., and Niu, X.: Retrieving high-resolution  
616 surface solar radiation with cloud parameters derived by combining MODIS and  
617 MTSAT data, Atmos. Chem. Phys., 16, 2543–2557, [https://doi.org/10.5194/acp-](https://doi.org/10.5194/acp-16-2543-2016)  
618 16-2543-2016, 2016.
- 619 Tang W., Yang, K., Qin, J., Niu, X., Lin, C., Jing, X.: A revisit to decadal change of  
620 aerosol optical depth and its impact on global radiation over China. Atmospheric



- 621 Environment, 150: 106-115, 2017a.
- 622 Tang, W., Yang, K., Sun, Z., Qin, J., and Niu, X.: Global Performance of a Fast  
623 Parameterization Scheme for Estimating Surface Solar Radiation From MODIS  
624 Data, IEEE T. Geosci. Remote Sens, 55, 3558–3571,  
625 <https://doi.org/10.1109/TGRS.2017.2676164>, 2017b.
- 626 Tang, W., Yang, K., Qin, J., Min, M., & Niu, X.: First Effort for Constructing a Direct  
627 Solar Radiation Data Set in China for Solar Energy Applications. Journal of  
628 Geophysical Research: Atmospheres, 123(3), 1724-1734.  
629 <https://doi.org/10.1002/2017jd028005>, 2018.
- 630 Tang, W., Yang, K., Qin, J., Li, X., & Niu, X.: A 16-year dataset (2000–2015) of high-  
631 resolution (3 h, 10 km) global surface solar radiation. Earth System Science Data,  
632 11(4), 1905-1915. <https://doi.org/10.5194/essd-11-1905-2019>, 2019a.
- 633 Tang, W., Li, J., Yang, K., Qin, J., Zhang, G., Wang, Y.: Dependence of remote sensing  
634 accuracy of global horizontal irradiance at different scales on satellite sampling  
635 frequency, Solar Energy, 193: 597–603, 2019b.
- 636 Tang, W. (2023). A dense station-based long-term and high-accuracy dataset of daily  
637 surface solar radiation in China. National Tibetan Plateau/Third Pole Environment  
638 Data Center, <https://doi.org/10.11888/Atmos.tpdc.300461>.
- 639 Wang, K. C., Dickinson, R. E., Wild, M., and Liang, S.: Atmospheric impacts on  
640 climatic variability of surface incident solar radiation, Atmos. Chem. Phys., 12,  
641 9581–9592, <https://doi.org/10.5194/acp-12-9581-2012>, 2012.
- 642 Wang, L., Kisi, O., Zounemat-Kermani, M., Salazar, G., Zhu, Z., & Gong, W.: Solar



- 643 radiation prediction using different techniques: Model evaluation and comparison.  
644 Renewable and Sustainable Energy Reviews, 61, 384–397.  
645 <https://doi.org/10.1016/j.rser.2016.04.024>, 2016.
- 646 Wild, M.: Global dimming and brightening: A review, *J. Geophys.Res.-Atmos.*, 888  
647 114, D00D16, 2009.
- 648 Wild, M., Folini, D., Hakuba, M.Z., et al.: The energy balance over land and oceans: an  
649 assessment based on direct observations and CMIP5 climate models. *Climate*  
650 *Dynamics*. 44, 3393-3429, 2015.
- 651 Wild, M., Ohmura, A., Schär, C., et al.: The Global Energy Balance Archive (GEBA)  
652 version 2017: A database for worldwide measured surface energy fluxes. *Earth*  
653 *System Science Data*. 9(2), 601-613, 2017.
- 654 Yang, X., Li, J., Yu, Q., et al.: Impacts of diffuse radiation fraction on light use  
655 efficiency and gross primary production of winter wheat in the North China Plain.  
656 *Agricultural and Forest Meteorology*, 275: 233-242, 2019.
- 657 Yang, K., Huang, G.-W., & Tamai, N.: A hybrid model for estimating global solar  
658 radiation. *Solar Energy*, 70(1), 13–22. [https://doi.org/10.1016/S0038-](https://doi.org/10.1016/S0038-092X(00)00121-3)  
659 [092X\(00\)00121-3](https://doi.org/10.1016/S0038-092X(00)00121-3), 2001.
- 660 Yang, K., Koike, T., & Ye, B.: Improving estimation of hourly, daily, and monthly  
661 downward shortwave radiation by importing global data sets. *Agricultural and*  
662 *Forest Meteorology*, 137(1-2), 43–55.  
663 <https://doi.org/10.1016/j.agrformet.2006.02.001>, 2006.
- 664 Yang, K., He, J., Tang, W., Qin, J., Cheng, C. C. K.: On downward shortwave and



665 longwave radiations over high altitude regions: Observation and modeling in the  
666 Tibetan Plateau, *Agricultural and Forest Meteorology*, 150(1): 38-46, 2010.

667 Zhang, X., Liang, S., Zhou, G., Wu, H., and Zhao, X.: Generating Global LAnd Surface  
668 Satellite incident shortwave radiation and photosynthetically active radiation  
669 products from multiple satellite data, *Remote Sens. Environ.*, 152, 318–332, 2014.

670 Zhang, Y. C., Rossow, W. B., Lacis, A. L., Valdar, O., and Michael, I. M.: Calculation  
671 of radiative fluxes from the surface to top of atmosphere based on ISCCP and other  
672 global data sets: refinements of the radiative transfer model and the input data, *J.*  
673 *Geophys. Res.*, 109, D19105, <https://doi.org/10.1029/2003JD004457>, 2004.